

# R-PINN: Recovery-type a-posteriori estimator enhanced adaptive PINN

Rongxin Lu<sup>a</sup>, Jiwei Jia<sup>a,b,\*</sup>, Young Ju Lee<sup>c</sup>, Zheng Lu<sup>a</sup>, Chensong Zhang<sup>d,e</sup>

<sup>a</sup>*Department of Computational Mathematics, School of Mathematics, Jilin University, Changchun, China*

<sup>b</sup>*Jilin National Applied Mathematical Center, Jilin University, Changchun, China*

<sup>c</sup>*Department of Mathematics, Texas State University, San Marcos, TX, USA*

<sup>d</sup>*LSEC and NCMIS, Academy of Mathematics and Systems Science, Beijing 100190, China*

<sup>e</sup>*School of Mathematical Sciences, University of Chinese Academy of Sciences, Beijing 100049, China*

---

## Abstract

In recent years, with the advancements in machine learning and neural networks, algorithms using physics-informed neural networks (PINNs) to solve PDEs have gained widespread applications. While these algorithms are well-suited for a wide range of equations, they often exhibit suboptimal performance when applied to equations with large local gradients, resulting in substantial localized errors. To address this issue, this paper proposes an adaptive PINN algorithm designed to improve accuracy in such cases. The core idea of the algorithm is to adaptively adjust the distribution of collocation points based on the recovery-type a-posteriori error of the current numerical solution, enabling a better approximation of the true solution. This approach is inspired by the adaptive finite element method. By combining the recovery-type a-posteriori estimator, a gradient-recovery estimator commonly used in the adaptive finite element method (FEM) with PINNs, we introduce the Recovery-type a-posteriori estimator enhanced adaptive PINN (R-PINN) and compare its performance with a typical adaptive PINN algorithm, FI-PINN. Our results demonstrate that R-PINN achieves faster convergence with fewer adaptive points and significantly outperforms in the cases with multiple regions of large errors than FI-PINN. Notably, our method is a hybrid numerical approach for solving partial differential equations, integrating adaptive FEM with PINNs.

*Keywords:*

Adaptive PINN, Recovery-type a-posteriori estimator, Machine learning, Adaptive FEM

---

## 1. Introduction

The Physics-informed neural networks (PINNs) algorithm is a data-driven approach for solving partial differential equations (PDEs) based on deep learning frameworks [1]. Due to its distinct methodology, which diverges significantly from traditional PDE numerical techniques, and by leveraging the superior capabilities of neural networks in handling large-scale data and optimization problems, PINNs have garnered considerable attention since their introduction and have become important tools for solving PDEs. These methods utilize

---

\*Corresponding author.

*Email address:* jiajiwei@jlu.edu.cn (Jiwei Jia)

automatic differentiation to compute the penalty of an equation at a set of collocation points within the domain of interest, using it as an objective loss function that is optimized through backpropagation, thereby approximating the solution of the PDE. Compared to classical PDE numerical methods such as the finite element method and finite difference method, one significant advantage of PINNs is that they are mesh-free, making them easier to implement and particularly well-suited for high-dimensional problems and irregular domains. Currently, PINNs have been applied to solve a range of PDE problems, demonstrating their strengths effectively, such as inverse problems in fluid dynamics, optics and metamaterials [2, 3], or some other forward problems [4, 5, 6].

Despite the notable advantages demonstrated by PINNs in PDEs, there remains substantial room for improvement in several aspects. While PINNs have exhibited high-precision solutions across a variety of scenarios, their applicability is still limited. Notably, significant errors can arise when addressing equations such as the Allen-Cahn equation or the Burgers' equation. Enhancements to the PINNs methodology can be pursued from multiple aspects. For instance, since the total loss function in PINNs is a weighted sum of errors from both the domain and boundary conditions, adjusting the weights of these terms may improve performance across different problems [7, 8, 9, 10]. In cases involving extensive solution domains, decomposition techniques can be employed to localize the training process, thereby enhancing optimization outcomes [11, 12, 13]. Regarding the choice of loss functions, although Mean Squared Error (MSE) is commonly used, alternative forms of loss functions may give better training results in certain circumstances [14, 10, 15]. Furthermore, strategies such as batch training and the design of specialized network architectures to deal with Dirichlet or periodic boundary conditions offer a promising direction to enhance the performance of PINNs [8, 16, 17]. In this paper, we focus on the limitations of PINNs in handling solutions with sharp local variations. This challenge, arising from singularities or high-gradient regions, is typically addressed by introducing adaptive sampling strategies for PINNs. However, existing sampling methods primarily only rely on the values of the loss function at local collocation points, without incorporating a rigorous a-posteriori error estimator. To address this issue, we propose the recovery-type a-posteriori estimator-enhanced adaptive PINN (R-PINN), which integrates the recovery-type a-posteriori estimator from classical numerical methods into PINNs. Furthermore, we introduce an adaptive sampling method, the Recovery-type estimator adaptive distribution (R-AD), to systematically implement adaptive refinement.

The sampling methods for collocation points in PINNs are generally categorized into uniform and non-uniform sampling. In typical uniform sampling, points are either randomly distributed or placed at equispaced intervals, remaining fixed throughout the training process. However, this static sampling strategy has notable limitations, as it fails to capture the model's fine local features effectively, which can lead to convergence issues in complex problems settings. To address these limitations, Lu et al. first proposed an adaptive non-uniform sampling method [18]. Since then, various adaptive sampling methods for collocation points have been developed [19, 20, 21, 22, 23, 24, 20]. Among these, the Failure-informed PINN (FI-PINN) by Gao et al. [20] is particularly notable, utilizing a truncated Gaussian model for adaptive sampling. Another significant contribution is by Wu et al. [19], who reviewed and compared a range of sampling techniques. Their work covers both uniform sampling methods, such as equispaced, random, and low-discrepancy sequences, and non-uniform

methods, including residual-based adaptive refinement (RAR) and residual-based adaptive distribution (RAD), offering valuable guidance on selecting appropriate sampling strategies.

While there are various adaptive PINN methods, they generally share a common approach: sampling the uniform points as background collocation points and then adding non-uniform points as the adaptive collocation points based on an a-posteriori error estimator. Most of these methods utilize the residual-type a-posteriori estimator, which calculates the error as the loss of the neural network function. For adaptive finite element methods, two primary types of estimator are widely recognized: residual-type [25, 26] and recovery-type [27, 28, 29], with the latter based on gradient recovery. Although extensive research has been conducted on adaptive PINNs, there has been limited work on gradient recovery estimators. Therefore, we introduce an adaptive PINN enhanced by the recovery-type a-posteriori estimator.

The rest of this paper is organized as follows. Section 2 provides preliminary background, introducing the fundamental algorithm of Physics-informed neural networks (PINNs) and existing sampling strategies for both uniform and non-uniform purposes. In Section 3, we present the detailed algorithm of the proposed Recovery-type estimator-enhanced PINN (R-PINN). Section 4 presents our results using R-PINN on four representative singular problems, illustrating its performance and providing a comparative analysis. Finally, Section 5 summarizes our conclusions and outlines potential directions for future research.

## 2. Preliminaries

In this section, we will present the requisite preliminary knowledge. We will begin with an overview of PINNs algorithm in solving both forward and inverse PDEs problems. Following this, we will discuss some strategies for collocation points sampling employed in the implementation of PINNs, including both uniform and non-uniform sampling methodologies.

### 2.1. PINNs for solving forward and inverse PDEs

Analogous to the application of basis functions for approximating true solutions in traditional numerical methods for PDEs, the Physics-informed neural networks (PINNs) algorithm utilizes deep neural networks to approximate the exact solutions of equations, primarily employing fully connected feed-forward neural networks. We denote a fully connected feed-forward neural network with  $L$  layers as  $\mathcal{N}^L : \mathbb{R}^{N_0} \rightarrow \mathbb{R}^{N_k}$ , where the  $k$ -th layer comprises  $N_k$  neurons. The weight matrix and bias vector of the  $k$ -th layer (for  $1 \leq k \leq L$ ) can be represented as  $\mathbf{W}^k \in \mathbb{R}^{N_k \times N_{k-1}}$  and  $\mathbf{b}^k \in \mathbb{R}^{N_k}$ , respectively. The input vector is denoted as  $\mathbf{x} \in \mathbb{R}^{N_0}$ , and the output vector of the  $k$ -th layer is expressed as  $\mathcal{N}^k(\mathbf{x})$ , especially,  $\mathcal{N}^0(\mathbf{x}) = \mathbf{x}$ . The activation function  $\Phi$ , applied during the feed-forward transition from the  $(k-1)$ -th layer to the  $k$ -th layer (for  $1 \leq k \leq L$ ), introduces non-linearity into the network, thereby enhancing its learning capacity. Consequently, a feed-forward neural network can be mathematically defined as

$$\mathcal{N}^k(\mathbf{x}) = \Phi(\mathbf{W}^k \mathcal{N}^{k-1}(\mathbf{x}) + \mathbf{b}^k), \quad 1 \leq k \leq L. \quad (2.1)$$

Letting  $\tilde{\Theta} = \{\mathbf{W}^k, \mathbf{b}^k\} \in \mathcal{V}$  be all parameters of the neural network, including weights and biases, where  $\mathcal{V}$  denotes the parameter space, we can finally express the neural network as

$$\hat{u}_{\tilde{\Theta}}(\mathbf{x}) = \mathcal{N}^L(\mathbf{x}; \tilde{\Theta}),$$

where  $\mathcal{N}^L(\mathbf{x}; \tilde{\Theta})$  emphasizes the dependence of the output layer  $\mathcal{N}^L(\mathbf{x})$  on  $\tilde{\Theta}$ . Initial parameters are typically generated according to a specified probability distribution.

In the context of solving PDEs with PINNs, we consider a PDE defined over the domain  $\Omega \in \mathbb{R}^d$  with parameters  $\boldsymbol{\lambda}$ ,

$$f(\mathbf{x}; u(\mathbf{x})) = f\left(\mathbf{x}; \frac{\partial u}{\partial x_1}, \dots, \frac{\partial u}{\partial x_d}; \frac{\partial^2 u}{\partial x_1^2}, \dots, \frac{\partial^2 u}{\partial x_1 \partial x_d}; \dots; \boldsymbol{\lambda}\right) = 0, \quad \mathbf{x} = (x_1, x_2, \dots, x_d) \in \Omega, \quad (2.2)$$

subject to the boundary condition:

$$\mathcal{B}(u, \mathbf{x}) = 0 \quad \text{on } \partial\Omega,$$

where  $u(\mathbf{x})$  represents the value of the true solution at point  $\mathbf{x}$ .

In solving the forward problem, where the parameter  $\boldsymbol{\lambda}$  in the equation is known, PINNs approximate the true solution  $u$  using a neural network  $\hat{u}_{\tilde{\Theta}}(\mathbf{x})$  [1]. During this process, the neural network is iteratively trained to update its parameters  $\tilde{\Theta}$  in order to minimize the loss function, defined as,

$$\mathcal{L}(\mathcal{T}; \tilde{\Theta}) = w_f \mathcal{L}_f(\mathcal{T}_f; \tilde{\Theta}) + w_b \mathcal{L}_b(\mathcal{T}_b; \tilde{\Theta}), \quad (2.3)$$

where

$$\begin{aligned} \mathcal{L}_f(\mathcal{T}_f; \tilde{\Theta}) &= \frac{1}{|\mathcal{T}_f|} \sum_{\mathbf{x} \in \mathcal{T}_f} \left| f\left(\mathbf{x}; \frac{\partial \hat{u}}{\partial x_1}, \dots, \frac{\partial \hat{u}}{\partial x_d}; \frac{\partial^2 \hat{u}}{\partial x_1 \partial x_1}, \dots, \frac{\partial^2 \hat{u}}{\partial x_1 \partial x_d}; \dots; \boldsymbol{\lambda}\right) \right|^2, \\ \mathcal{L}_b(\mathcal{T}_b; \tilde{\Theta}) &= \frac{1}{|\mathcal{T}_b|} \sum_{\mathbf{x} \in \mathcal{T}_b} |\mathcal{B}(\hat{u}, \mathbf{x})|^2, \end{aligned} \quad (2.4)$$

and  $w_f$  and  $w_b$  are weighting factors. Here,  $\mathcal{T}_f$  and  $\mathcal{T}_b$  denote the sets of sampled points within the domain and on the boundary, respectively, which are commonly referred to as "collocation points". The combined set of collocation points is given by  $\mathcal{T} = \mathcal{T}_f \cup \mathcal{T}_b$ .

For certain problems, while the parameters  $\boldsymbol{\lambda}$  in the governing equations remain unknown, the solutions are observable, thereby giving rise to inverse problems. To solve the inverse problem with PINNs, the loss function not only accounts for the deviations dictated by physical laws but also incorporates an additional term to capture the residual between observed solution  $u(\mathbf{x})$  and predicted solution  $\hat{u}(\mathbf{x})$  over a set of collocation points  $\mathcal{T}_i$ :

$$\mathcal{L}_i(\mathcal{T}_i; \tilde{\Theta}, \boldsymbol{\lambda}) = \frac{1}{|\mathcal{T}_i|} \sum_{\mathbf{x} \in \mathcal{T}_i} |\hat{u}(\mathbf{x}) - u(\mathbf{x})|^2. \quad (2.5)$$

As a result, the total loss function for the inverse problem can be expressed as:

$$\mathcal{L}(\mathcal{T}; \tilde{\Theta}, \boldsymbol{\lambda}) = w_f \mathcal{L}_f(\mathcal{T}_f; \tilde{\Theta}, \boldsymbol{\lambda}) + w_b \mathcal{L}_b(\mathcal{T}_b; \tilde{\Theta}, \boldsymbol{\lambda}) + w_i \mathcal{L}_i(\mathcal{T}_i; \tilde{\Theta}, \boldsymbol{\lambda}), \quad (2.6)$$

with the weight of the additional term  $w_i$ . Then the unknown parameters  $\boldsymbol{\lambda}$  can be trained with the neural network parameters  $\tilde{\Theta}$  by the optimization process.

Note that in equations (2.3) and (2.6), it is crucial to position the set of collocation points within the domain of interest. While simple sampling methods, such as uniform and random sampling, are available, they are generally less effective in capturing the solution's local features. Consequently, in certain cases, employing more advanced non-uniform sampling techniques becomes particularly important.

## 2.2. Sampling methods for PINNs

Typically, the sampling strategy in PINNs involves selecting a set of collocation points by uniform sampling prior to training the neural network, with the set remaining fixed throughout the training process. Commonly employed uniform sampling methods include equispaced uniform sampling and uniformly random sampling, while other uniform sampling techniques are also available [1, 4, 30]. In Wu. et al.’s work [19], six uniform sampling methods were systematically reviewed, including equispaced uniform grid (Grid), uniformly random sampling (Random), Latin hypercube sampling (LHS) [31, 32], Halton sequence (Halton) [33], Hammersley sequence (Hammersley) [34], and Sobol sequence (Sobol) [35]. Their comparative experiments demonstrated that the Sobol method generally provides superior performance. The Sobol sequence uses a base of two to form successively finer uniform partitions of the unit interval and then reorder the coordinates in each dimension. We show the difference over three different methods in Fig. 1.

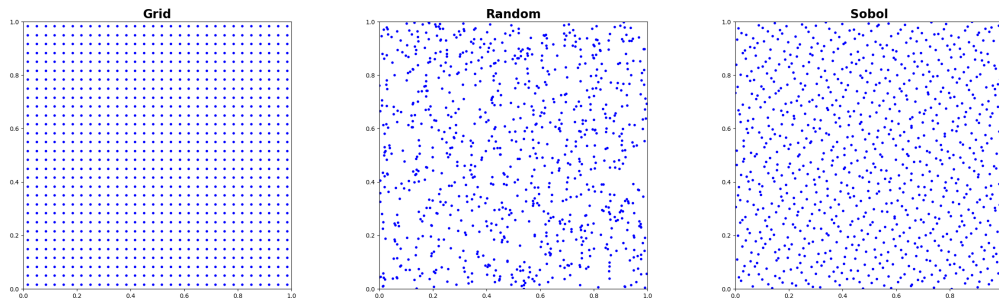


Fig. 1: 900 uniformly collocation points generated on  $[0, 1]^2$  with three different strategies.

In many cases, accuracy of numerical solution can be enough through uniform sampling strategies. However, for certain numerical problems characterized by large local gradients and highly distinctive solution features, such methods may fail to adequately capture local variations. Several adaptive methods have been proposed to overcome these limitations in recent years, primarily through modifications to the sampling strategies for the collocation points in PINNs. These adaptive sampling approaches can be broadly categorized into two types [19]: the Residual-based adaptive refinement (RAR) [18] and the Residual-based adaptive distribution (RAD) [21]. RAR targets regions with large residuals, where new adaptive collocation points are introduced at regular intervals during the training process to reduce local errors (see Algorithm 1).

While RAR only focuses on the area with large residuals and ignore the other place, RAD utilizes the probability density function  $p(\mathbf{x})$  that has strong relationship with residual to resample all the collocation points, which can take the area both with large and small residual into care (see Algorithm 2). For example, we can take  $p(\mathbf{x})$  proportional to the PDE residual  $\epsilon(\mathbf{x}) = |f(\mathbf{x}; \hat{u}(\mathbf{x}))|$ ,

$$p(\mathbf{x}) = \frac{\epsilon(\mathbf{x})}{A}, \quad A = \int_{\Omega} \epsilon(\mathbf{x}) \, d\mathbf{x}. \quad (2.7)$$

---

**Algorithm 1** Residual-based adaptive refinement (RAR)

---

- 1: Sample background collocation points  $\mathcal{T}$ .
  - 2: Train the neural network with  $\mathcal{T}$  for a certain number of epoches.
  - 3: **while** not reach the end **do**
  - 4:   Sample a set of adaptive collocation points  $\mathcal{S}_0$ .
  - 5:   Compute the PDE residuals of adaptive collocation points  $\mathcal{S}_0$ .
  - 6:    $S \leftarrow m$  points with largest residuals from  $\mathcal{S}_0$ .
  - 7:    $\mathcal{T} \leftarrow \mathcal{T} \cup S$ .
  - 8:   Train the neural network for some epoches.
  - 9: **end while**
  - 10: Output the result.
- 

More forms of  $p(x)$  can be used here, such as it in paper[19],

$$p(\mathbf{x}) \propto \frac{\epsilon^k(\mathbf{x})}{\mathbb{E}[\epsilon^k(\mathbf{x})]} + c, \quad (2.8)$$

where  $k \geq 0, c \geq 0$  are two hyperparameters.

---

**Algorithm 2** Residual-based adaptive distribution (RAD)

---

- 1: Sample background collocation points  $\mathcal{T}$ .
  - 2: Train the neural network with  $\mathcal{T}$  for a certain number of epoches.
  - 3: **while** not reach the end **do**
  - 4:    $\mathcal{T} \leftarrow$  resampled collocation points according to the probability density function  $p(\mathbf{x})$ .
  - 5:   Train the neural network for some epoches.
  - 6: **end while**
  - 7: Output the result.
- 

### 3. Recovery-type estimator enhanced PINN

In this section, we present an adaptive PINNs algorithm developed by our team, which utilizes the recovery-type a-posteriori error estimator [27, 28, 29], a widely used technique in adaptive finite element methods. The concept of adaptive finite element method, first introduced by I. Babuška et al. in 1978 [25], has since seen significant advancements and remains integral to practical scientific computations. This approach extends classical finite element methods by incorporating a-posteriori error estimation and automated mesh refinement to iteratively improve the accuracy of approximate solutions, which can achieve the target accuracy with reduced computational effort, offering distinct advantages over traditional finite element methods, particularly when addressing problems involving singular solutions.

The fundamental concept of the adaptive finite element method lies in the use of a-posteriori error estimator to assess the numerical solution error within each mesh element, thereby guiding the mesh refinement and coarsening process. This adaptive mesh strategy shares a notable similarity with adaptive PINNs, where the distribution of collocation points

is adjusted based on the error distribution. In adaptive finite element methods, commonly employed a-posteriori error estimators can be categorized into two main types: the first is based on residual type [25, 36], where the error is estimated by computing the discrepancy between the solution and the residual of the governing equation; the second type, recovery type, proposed by the Zienkiewicz and Zhu [27, 28, 29], is a gradient reconstruction-based method that provides more accurate error estimates by reconstructing the solution gradients.

In existing adaptive PINNs algorithms, the equation operator is typically used as the default a-posteriori error estimator, which corresponds to the residual-based error estimator in adaptive finite element methods. Our proposed algorithm seeks to introduce the recovery-type error estimator into the adaptive PINNs framework, with the aim of enriching and extending the theoretical foundation of adaptive PINNs, ultimately providing a more comprehensive approach to error estimation and control.

### 3.1. Recovery-type a-posteriori estimator

In 1987, O.C. Zienkiewicz and J.Z. Zhu introduced a pioneering a-posteriori error estimator based on gradient recovery for finite element theory, commonly referred to as the Z-Z method [27] or the recovery-type method. This approach, notable for its computational simplicity, intuitive understanding, and straightforward implementation within finite element software, quickly gained widespread acceptance within the engineering community. Its rapid adoption represented a significant milestone, facilitating the transition from theoretical research to practical application in the domain of finite element a-posteriori error estimation.

In the context of a specific recovery-type a-posteriori error estimation framework, a typical problem in the field of elasticity is to be considered as an example, which is encapsulated within the following system of equations

$$\mathbf{L}u = \mathbf{S}^T \mathbf{D} \mathbf{S} u = \mathbf{f} \quad \text{in } \Omega, \quad (3.1)$$

which is subject to suitable boundary conditions on the domain's boundary  $\partial\Omega$ . Here,  $\mathbf{u}$  represents the displacement vector,  $\mathbf{L}$  is the differential operator intrinsic to the theory of elasticity, and the matrix operator  $\mathbf{S}$  defines the strain tensor  $\boldsymbol{\epsilon}$  by

$$\boldsymbol{\epsilon} = \mathbf{S}u. \quad (3.2)$$

Furthermore, the elasticity matrix  $\mathbf{D}$  is utilized to determine the stress tensor  $\boldsymbol{\sigma}$ , as delineated by the equation:

$$\boldsymbol{\sigma} = \mathbf{D}\boldsymbol{\epsilon}. \quad (3.3)$$

The finite element solution to the aforementioned elasticity problem is expressed in the following form

$$\mathbf{u}_h = \mathbf{N}\bar{\mathbf{u}}_h, \quad (3.4)$$

where  $\bar{\mathbf{u}}_h$  denotes the vector of nodal displacements, and  $\mathbf{N}$  represents the set of approximate polynomial shape functions that interpolate the displacement field within the finite element framework. Subsequently, the stress tensor  $\boldsymbol{\sigma}_h$ , is computed using the approximate displacement field  $\mathbf{u}_h$  with

$$\boldsymbol{\sigma}_h = \mathbf{D}\mathbf{S}\mathbf{u}_h. \quad (3.5)$$

The recovery-type a-posteriori error estimator is characterized by focusing on estimating the numerical error by approximating the gradient recovery of the numerical solution  $\sigma^*$ . Therefore, the gradient recovery technique plays a key role for the estimator. With the development of recovery-type a-posteriori error estimators, there have been many gradient recovery methods, the typical ones are the transformation method and nodal averaging method.

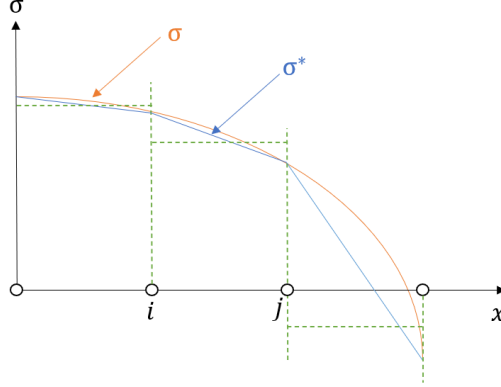


Fig. 2: The finite element method solution and the smoothed solution of stress for a one-dimensional problem.

- The transformation method

For this method, it is assumed that the stress

$$\sigma^* = \mathbf{N} \bar{\sigma}^*, \quad (3.6)$$

and the method seeks to minimize the discrepancy between the smooth stress  $\sigma^*$  and the stress of the finite element  $\sigma_h$  by enforcing the condition

$$\int_{\Omega} \mathbf{N}^T (\sigma^* - \sigma_h) d\Omega = 0. \quad (3.7)$$

By combining equations (3.6) and (3.7), we can derive the following expression for  $\bar{\sigma}^*$

$$\bar{\sigma}^* = \mathbf{A}^{-1} \int_{\Omega} \mathbf{N}^T \mathbf{D} \mathbf{S} \mathbf{N} d\Omega \cdot \bar{\mathbf{u}}_h, \quad \mathbf{A}^{-1} = \int_{\Omega} \mathbf{N}^T \mathbf{N} d\Omega \quad (3.8)$$

This method is highly accurate but computationally expensive due to the need to solve the additional system of equations.

- The nodal averaging method

In this simpler approach, the smooth stress  $\bar{\sigma}^*$  is obtained by averaging the finite element stresses  $\sigma_{h,i}$  at the nodes

$$\sigma^* = \frac{\left( \sum_{i=1}^M \sigma_{h,i} \right)}{M} \quad (3.9)$$

where  $M$  is the number of elements connected with the node  $i$ .

This method is straightforward and computationally efficient, although it may not achieve the same level of accuracy as the transformation method. Nevertheless, it performs well in practical applications.

As for error estimation, two types of errors are usually considered. One is the error in  $\boldsymbol{\sigma}$  which can be expressed as

$$\|\mathbf{e}_\sigma\| = \|\boldsymbol{\sigma} - \boldsymbol{\sigma}_h\|. \quad (3.10)$$

The other is the recovery-type estimator of the error is similarly defined in the appropriate norm as

$$\|\tilde{\mathbf{e}}_\sigma\| = \|\boldsymbol{\sigma}^* - \boldsymbol{\sigma}_h\|, \quad (3.11)$$

and its efficiency is gauged by the efficacy index defined as

$$\theta = \frac{\|\tilde{\mathbf{e}}_\sigma\|}{\|\mathbf{e}_\sigma\|}. \quad (3.12)$$

The confines of this efficacy index are elucidated through the subsequent theorem (as detailed in [29]):

$$1 - \frac{\|\mathbf{e}_\sigma^*\|}{\|\mathbf{e}_\sigma\|} \leq \theta \leq 1 + \frac{\|\mathbf{e}_\sigma^*\|}{\|\mathbf{e}_\sigma\|}, \quad (3.13)$$

with the error in the reconstructed solution characterized as

$$\|\mathbf{e}_\sigma^*\| = \|\boldsymbol{\sigma} - \boldsymbol{\sigma}^*\|. \quad (3.14)$$

It is evident that the efficacy index approaches unity when the precision of the reconstructed solution significantly outperforms that of the original finite element solution.

Should the reconstructed solution exhibit superconvergence, that is,

$$\|\mathbf{e}_\sigma^*\| = C^* h^{p+\alpha}, \quad (3.15)$$

where  $\alpha$  is a positive constant and  $h$  represents the element size, and

$$\|\mathbf{e}_\sigma\| = Ch^p, \quad (3.16)$$

then the bounds for the efficacy index are

$$1 - \tilde{C}h^\alpha \leq \theta \leq 1 + \tilde{C}h^\alpha, \quad (3.17)$$

with  $\tilde{C} = C^*/C$ , rendering the error estimator asymptotically precise. This estimation underscores the efficiency of the recovery-type a-posteriori estimator. Given that the error estimation revolves around stress  $\boldsymbol{\sigma}$ , which is contingent upon the gradients of the solution  $\mathbf{u}$ , this class of estimator may also be regarded as a form of gradient recovery.

### 3.2. Algorithm of Recovery-type estimator enhanced PINN

In this section, we introduce the algorithm of recovery-type estimator enhanced adaptive PINN (R-PINN). The success of the adaptive PINNs algorithm hinges on two crucial components: the posterior error estimation method and the adaptive sampling strategy. The posterior error estimation predicts the discrepancy between the numerical and true solutions, while the adaptive sampling strategy adjusts the distribution of collocation points based on this error, allowing for more focused and efficient training in areas that need it most. Section 3.1 provides a comprehensive explanation of the posterior error estimation method. Therefore, for our R-PINN, the key is how to combine PINNs with this kind of posterior error estimator to realize the adaptive process.

To solve the equation (2.2), we utilize a shape-regular triangulation  $\mathcal{T}_h$  formed by a family of partitions of the domain  $\Omega$ , which allows us to effectively implement the recovery-type a-posteriori estimator. We define the operator  $\mathcal{P}(\hat{u}_{\hat{\Theta}}, \mathcal{T}_h)$  as the recovery-type estimator used in our algorithm, employing a nodal averaging method for gradient recovery (other gradient recovery methods can also be utilized). The approximated solution  $\hat{u}_{\hat{\Theta}}$  predicts the solution values at all nodes within the mesh  $\mathcal{T}_h$ , which then facilitates gradient recovery and error computation for each element  $K \in \mathcal{T}_h$  through the recovery-type operator  $\mathcal{P}(\hat{u}_{\hat{\Theta}}, \mathcal{T}_h)$ .

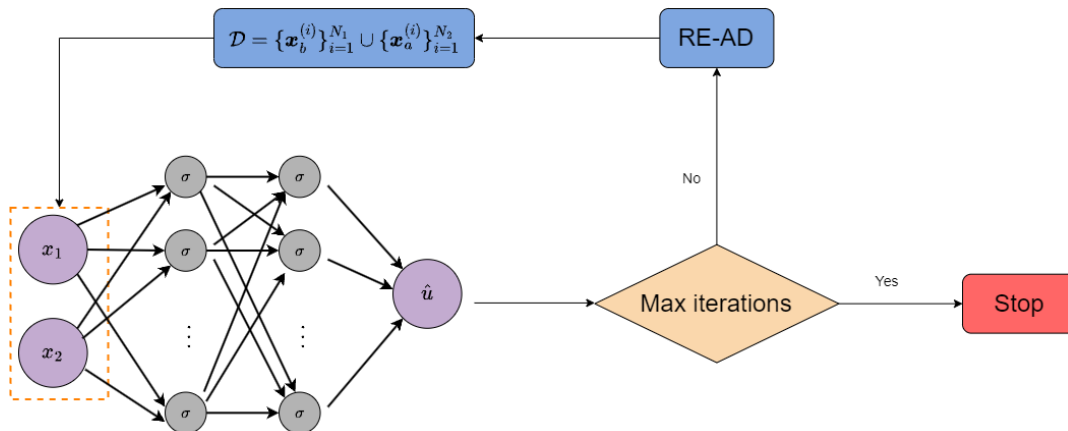


Fig. 3: The flow chart of R-PINN.

Another crucial aspect is the selection of collocation points and the adaptive adjustment of their distribution. Similar to many adaptive PINNs algorithms, we start with  $N_1$  background collocation points  $\{\mathbf{x}_b^{(i)}\}_{i=1}^{N_1}$  for pre-training. During the adaptive training phase, we introduce  $N_2$  adaptive collocation points  $\{\mathbf{x}_a^{(i)}\}_{i=1}^{N_2}$  alongside the background collocation points  $\{\mathbf{x}_b^{(i)}\}_{i=1}^{N_1}$ , updating the adaptive collocation points after each training batch. For background collocation points, we utilize a Sobol sequence as described in section 2.2. For the adaptive collocation points, we propose a novel approach called the recovery-type estimator based adaptive distribution (RE-AD).

Unlike common sampling methods, the RE-AD technique is element-based, as the computed a-posteriori errors are distributed across elements. This means we only need to specify the number of adaptive collocation points to sample in each element, allowing for random sampling within each element. Therefore, it's vital to allocate adaptive collocation points intelligently to target areas with significant errors without creating redundancy. To achieve

this, we design an iterative process: we define a tolerance  $\epsilon$  such that  $\frac{N_2}{N_e} \leq \epsilon < 1$ , where  $N_e$  is the total number of elements. Initially, we select  $L_1 = \lceil \epsilon N_e \rceil$  elements that exhibit the largest errors in  $\mathcal{T}_h$ , which we refer to as the sequence  $\mathcal{S}_1$ . Adaptive collocation points are sampled from  $\mathcal{S}_1$  in proportion to the errors. For instance, for the  $i$ -th element in  $\mathcal{S}_1$ , the number of adaptive collocation points assigned is  $\lfloor N_2 \frac{e_i}{\sum_j e_j} \rfloor$ . Since this process rounds down, some adaptive collocation points may remain unallocated. We then repeat this process by selecting  $L_2 = \lceil \epsilon L_1 \rceil$  of the largest elements and allocating adaptive collocation points according to their errors, continuing until no points are redundant. The RE-AD sampling method differs from RAR but is more akin to RAD, as it maintains a fixed total number of adaptive collocation points while only adjusting their distribution during each iteration.

---

**Algorithm 3** Recovery-type estimator based adaptive distribution (RE-AD)

---

- 1: Set the number of redundant adaptive collocation points  $N_r = N_2$ .
  - 2: Denote  $L_0 = N_e$ .
  - 3:  $k \leftarrow 1$ .
  - 4: **while**  $N_r$  not 0 **do**
  - 5:   Select  $L_k = \lceil \epsilon L_{k-1} \rceil$  elements with the largest errors as  $\mathcal{S}_k$ .
  - 6:   Designate adaptive collocation points to  $\mathcal{S}_k$ .
  - 7:   Update the number of redundant adaptive collocation points  $N_r$ .
  - 8:    $k \leftarrow k + 1$ .
  - 9: **end while**
  - 10: Output adaptive collocation points  $\{\mathbf{x}_a\}_{i=1}^{N_2}$ .
- 

To introduce the specific procedures of the recovery-type estimator enhanced adaptive PINN (R-PINN), we utilize the recovery-type operator  $\mathcal{P}(\hat{u}_{\tilde{\Theta}}, \mathcal{T}_h)$  along with the recovery-type estimator based adaptive distribution (RE-AD) sampling strategy. Initially, we use a set of background collocation points  $\{\mathbf{x}_b^{(i)}\}_{i=1}^{N_1}$  to train the neural network, aiming to obtain a rough approximation of the true solution, which serves as the pre-training step. Following the pre-training phase, an adaptive training iteration process begins. In each iteration, the recovery-type operator  $\mathcal{P}(\hat{u}_{\tilde{\Theta}}, \mathcal{T}_h)$  is used to compute the errors of the approximated solution  $\hat{u}_{\tilde{\Theta}}(\mathbf{x})$  on the mesh  $\mathcal{T}_h$ . Based on these errors, the RE-AD sampling method is then employed to strategically distribute additional adaptive collocation points. These adaptive collocation points are combined with the background collocation points to retrain the neural network. This iterative process continues until the accuracy improvements become minimal, indicating that the network has converged to a satisfactory approximation of the solution. Since the number of collocation points can always stay constant, the algorithm satisfies the characteristics of self-adaptation while ensuring accurate solution.

## 4. Numerical experiments

In this section, we present numerical experiments demonstrating the effectiveness of our proposed algorithm. Our evaluation compares three different kinds of PINNs: the Recovery-type estimator enhanced PINN (R-PINN), Failure-informed PINN (FI-PINN) [20], and standard PINN as a baseline.

---

**Algorithm 4** Recovery-type estimator enhanced PINN (R-PINN)

---

**Require:** The number of adaptive samples and background samples  $N_a$  and  $N_b$ , the maximum steps number  $M$

- 1: Generate  $N_1$  background samples  $\{\mathbf{x}_b^{(i)}\}_{i=1}^{N_1}$  with Sobol sequence.
  - 2: Pre-train the network  $\hat{u}_{\tilde{\Theta}}(\mathbf{x}) = \mathcal{N}^L(\mathbf{x}; \tilde{\Theta})$  with background samples  $\{\mathbf{x}_b^{(i)}\}_{i=1}^{N_1}$ .
  - 3: Set the number of iteration  $k \leftarrow 1$  and give the max number of iterations  $M$ .
  - 4: **while**  $k \leq M$  **do**
  - 5:   Generate  $N_2$  adaptive samples  $\{\mathbf{x}_a^{(i)}\}_{i=1}^{N_2}$  with RE-AD method.
  - 6:   Retrain the network  $\hat{u}_{\tilde{\Theta}}(\mathbf{x}) = \mathcal{N}^L(\mathbf{x}; \tilde{\Theta})$  with the dataset  $\mathcal{D} = \{\mathbf{x}_b^{(i)}\}_{i=1}^{N_1} \cup \{\mathbf{x}_a^{(i)}\}_{i=1}^{N_2}$ .
  - 7: **end while**
  - 8: **return** approximated solution  $\hat{u}_{\tilde{\Theta}}(\mathbf{x}) = \mathcal{N}^L(\mathbf{x}; \tilde{\Theta})$ .
- 

#### 4.1. Experimental setup

To ensure a fair comparison, we maintain identical parameters and training processes across all methods for the same number of iterations, varying only the number and distribution of adaptive collocation points. The recovery-type a-posteriori estimation is implemented using *FEALPy* [37].

All experiments employ a fully-connected neural network with 7 hidden layers, each containing 20 neurons with *tanh* for the activation function unless otherwise specified. The training process comprises two phases: an initial pre-training phase utilizing the *L-BFGS* optimizer with a learning rate of 0.1, conducted for a problem-dependent number of epochs, followed by an adaptive training phase consisting of  $M$  adaptive iterations. Each iteration is constrained to 5000 epochs while employing the same optimization method.

For collocation points, we use  $N_1 = 2000$  background collocation points and  $N_2 = 100$  adaptive collocation points for R-PINN unless specified, while FI-PINN requires  $N_2 = 500$  adaptive collocation points to achieve convergence unless specified. For the standard PINN, only  $N_1 = 2000$  background collocation points are used during training, without incorporating additional adaptive collocation points. However, the training process remains the same as that of the two adaptive PINNs, with each adaptive iteration also consisting of 5000 epochs. All methods utilize 200 boundary collocation points. Notably, our approach achieves comparable or superior accuracy despite using fewer total epochs and adaptive collocation points than related studies. The larger  $N_2$  value for FI-PINN is necessary as it fails to achieve adaptivity with fewer points. Furthermore, while our method maintains a fixed number of adaptive collocation points, FI-PINN accumulates points throughout the adaptive iteration process. To evaluate the accuracy of our method, we employ two error metrics: the relative  $L^2$  error,

$$\frac{\|\hat{u}_{\tilde{\Theta}} - u\|_2}{\|u\|_2}, \quad (4.1)$$

and the  $L^\infty$  error, defined as  $\|\hat{u}_{\tilde{\Theta}} - u\|_\infty$ . Here,  $\hat{u}_{\tilde{\Theta}}$  denotes the numerical solution obtained by our method, and  $u$  represents the exact solution.

#### 4.2. Poisson equation

Consider the following Poisson equation:

$$\begin{aligned} -\Delta u(x, y) &= f(x, y), & (x, y) \text{ in } \Omega, \\ u(x, y) &= g(x, y), & (x, y) \text{ on } \partial\Omega, \end{aligned} \tag{4.2}$$

where the domain  $\Omega$  is  $= [0, 1] \times [0, 1]$ , and the true solution is

$$u(x, y) = e^{-1000[(x-0.5)^2+(y-0.5)^2]}. \tag{4.3}$$

The solution exhibits a sharp peak near the point  $(0.5, 0.5)$ , which is challenging for standard PINN to capture accurately. In this experiment, we pre-train the network for 10000 iterations and set the maximum number of adaptive iterations to  $M = 5$ .

$N_{\text{iter}}$	R-PINN			FI-PINN			standard PINN	
	Relative $L^2$	$L^\infty$	$N_2$	Relative $L^2$	$L^\infty$	$N_2$	Relative $L^2$	$L^\infty$
1	3.386	0.0990	100	2.717	0.6541	500	0.809	0.6270
2	0.732	0.0282	100	1.514	0.4593	1000	0.689	0.6180
3	0.125	0.0260	100	1.157	0.3095	1500	0.650	0.5683
4	0.285	0.0088	100	0.294	0.0686	2000	0.879	0.5689
5	0.139	0.0086	100	0.068	0.0335	2500	0.682	0.5570

Table 1: The relative  $L^2$  error and  $L^\infty$  error by two methods solving Poisson equation.

Fig. 4 illustrates the distribution of adaptive collocation points by two adaptive methods in the first two adaptive iterations. It is evident that all adaptive collocation points of our model converge to the neighborhood of the point  $(0.5, 0.5)$ , while adaptive collocation points of FI-PINN are more dispersed. This shows the strong effectiveness of our algorithm in handling problems with significant local variations. Table 1 compares the relative  $L^2$  error and  $L^\infty$  error among R-PINN, FI-PINN and standard PINN during the adaptive iterations where  $N_{\text{iter}}$  represents the number of adaptive iterations. The relative  $L^2$  error for R-PINN reaches 0.139, and the  $L^\infty$  error reaches 0.0086. In contrast, the errors obtained by FI-PINN decrease slowly at the beginning, but drop fast later, reaching the relative  $L^2$  error of 0.068 and  $L^\infty$  error of 0.0335. It can be observed that R-PINN can converge faster than FI-PINN. While, R-PINN can reach a smaller relative  $L^2$  error in this case with the exponentially accumulated adaptive collocation points, which is one of its advantage. As for the normal PINN, the errors obtained show little to no decrease, indicating that the normal PINN fails to converge effectively. Similar results are observed in Fig. 6, where the lowest relative  $L^2$  error for our algorithm is below  $1 \times 10^{-1}$ . In the left panel of Fig. 5, we show the absolute errors throughout the entire domain, clearly demonstrating that the errors are much smaller with R-PINN. The middle panel of Fig. 5 illustrates the cross-section at  $y = 0.5$ . The predicted curve using R-PINN fits the true solution very well, while the solution by FI-PINN has a little obvious error at the foot of the peak. The final solutions with three methods are plotted in the right of Fig. 5.

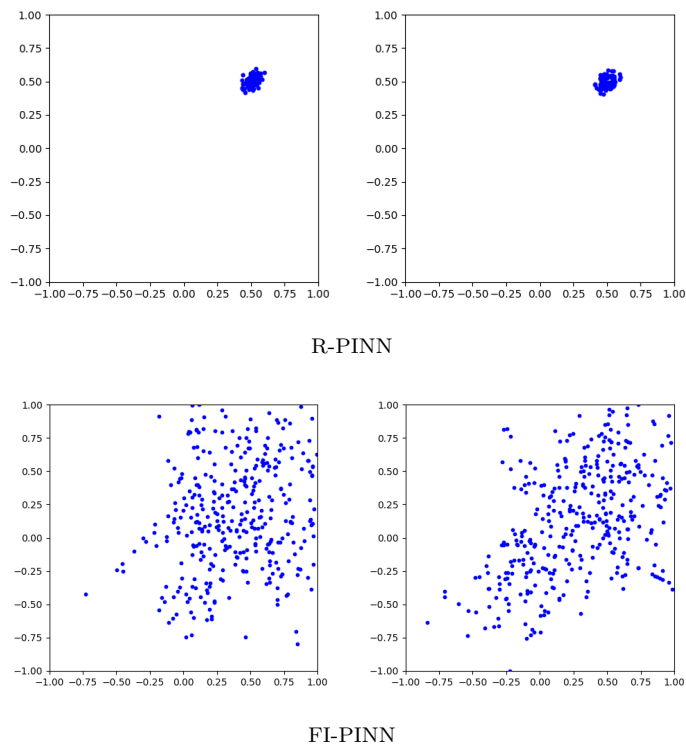


Fig. 4: The distribution of adaptive collocation points in the first 2 adaptive iterations with two adaptive PINN methods.

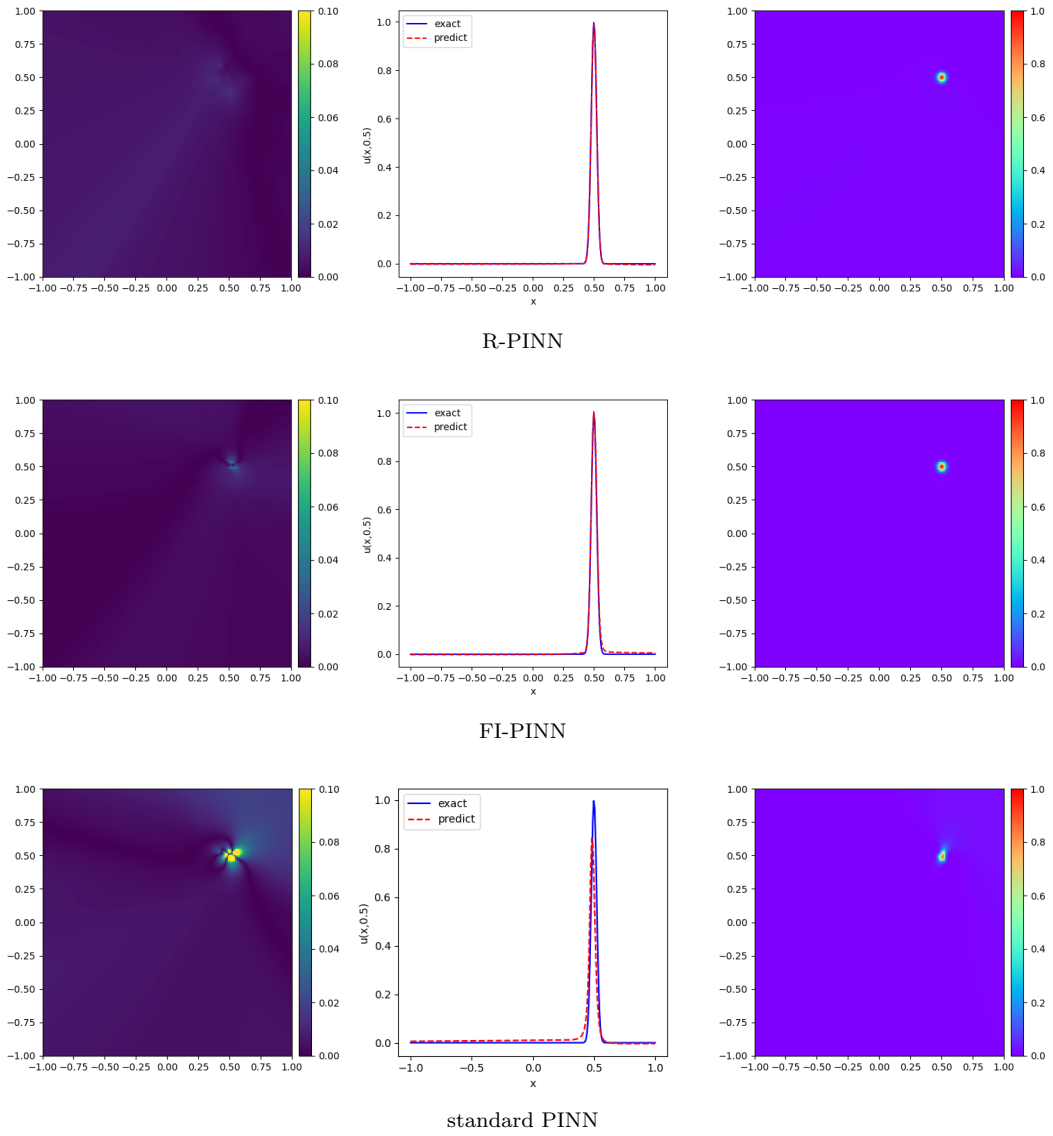


Fig. 5: The prediction err (left), the cross section at  $y = 0.5$  (middle) and the predicted solution of three methods solving Poisson equation.

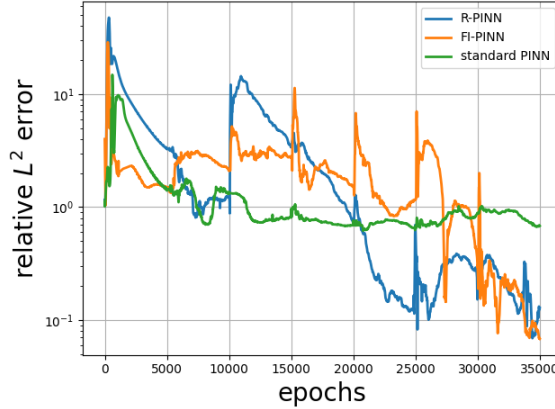


Fig. 6: The relative  $L^2$  errors of three methods in the optimization process of solving Poisson equation.

### 4.3. Burgers' equation

We consider the following Burgers' equation:

$$\begin{aligned} \frac{\partial u}{\partial t} + u \frac{\partial u}{\partial x} &= \frac{0.01}{\pi} \frac{\partial^2 u}{\partial x^2}, \\ u(x, 0) &= -\sin(\pi x), \\ u(t, -1) = u(t, 1) &= 0 \end{aligned} \quad (4.4)$$

where the domain is  $(x, t) \in [-1, 1] \times [0, 1]$ . The solution to this Burgers' equation exhibits a sharp mutation along  $x = 0$ , making it prone to errors and offsets. For this test, we pre-train the network for 5000 iterations and use  $M = 4$  steps of adaptive processes.

$N_{\text{iter}}$	R-PINN			FI-PINN			standard PINN	
	Relative $L^2$	$L^\infty$	$N_2$	Relative $L^2$	$L^\infty$	$N_2$	Relative $L^2$	$L^\infty$
1	0.0086	0.0735	100	0.2278	1.8142	200	0.0136	0.1583
2	0.0107	0.0964	100	0.0131	0.1263	400	0.0144	0.1685
3	0.0071	0.0673	100	0.0064	0.0576	600	0.0174	0.2099
4	0.0059	0.0439	100	0.0089	0.0846	800	0.0197	0.2418

Table 2: The relative  $L^2$  error and  $L^\infty$  error by three methods solving Burgers' equation.

The adaptive collocation points generated during the first two adaptive training processes by two adaptive PINN method are illustrated in Fig. 7. We observe that the adaptive collocation points successfully cluster around  $x = 0$  with both methods, where the error is largest (as seen in Fig. 8). This clustering significantly improves the local error. The exact relative  $L^2$  error and  $L^\infty$  error are listed in Table 2. As shown, the final relative  $L^2$  error and  $L^\infty$  error for R-PINN are 0.0059 and 0.0439, respectively, while those for FI-PINN are 0.0089 and 0.0846. The prediction err of standard PINN keeps at the save level during the training, where relative  $L^2$  error and  $L^\infty$  reach 0.0197 and 0.2418 in the final. Similar to the experiment of Poisson equation, it takes a long iterations for FI-PINN before the error jumps quickly, while R-PINN can reduce the errors at once. The errors obtained by

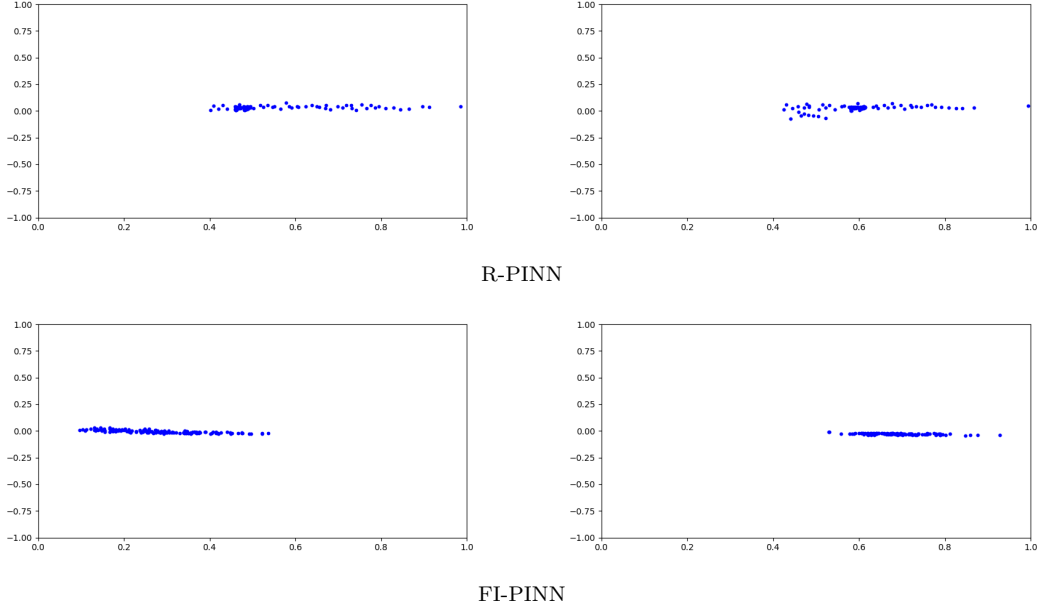


Fig. 7: The distribution of adaptive collocation points in the first 2 adaptive iterations with two adaptive PINN methods solving Burgers' equation.

R-PINN and FI-PINN are one order of magnitude lower than those obtained by the standard PINN. Such behaviour can also be observed in the Fig. 10, where the relative  $L^2$  errors are illustrated specifically, showing that the lowest error can reach below  $1 \times 10^{-2}$ . We also show the absolute errors across the entire domain and the cross-section at  $t = 1$  in Fig. 8. The predicted solutions of two adaptive methods are illustrated in Fig. 9.

#### 4.4. Two-dimensional problem with two peaks

Considering the following two-dimensional problem

$$\begin{aligned} -\nabla \cdot [u(x, y)\nabla(x^2 + y^2)] + \nabla^2 u(x, y) &= f(x, y), & (x, y) \in \Omega, \\ u(x, y) &= b(x, y), & (x, y) \in \partial\Omega, \end{aligned} \quad (4.5)$$

where  $\Omega = [-1, 1] \times [-1, 1]$ . The true solution is

$$u(x, y) = e^{-1000[(x-0.5)^2+(y-0.5)^2]} + e^{-1000[(x+0.5)^2+(y+0.5)^2]}, \quad (4.6)$$

which has two peaks at  $(-0.5, -0.5)$  and  $(0.5, 0.5)$ . This test mainly can show the ability of R-PINN to deal with multiple peaks. For this experiment, we pre-train our network for the period of 10000 iterations and set the maximum number of adaptive iterations as  $M = 4$ . Since two peaks problem is challenging for neural network to approximate, we use 5 hidden layers with 64 neurons in each layer to enhance its capability. Moreover, we use  $N_2 = 150$  adaptive collocation points for R-PINN, and  $N_2 = 750$  added adaptive collocation points for FI-PINN.

We present the distribution of adaptive collocation points of two adaptive methods across the first two adaptive iterations in Fig. 11. It is evident that these points converge around

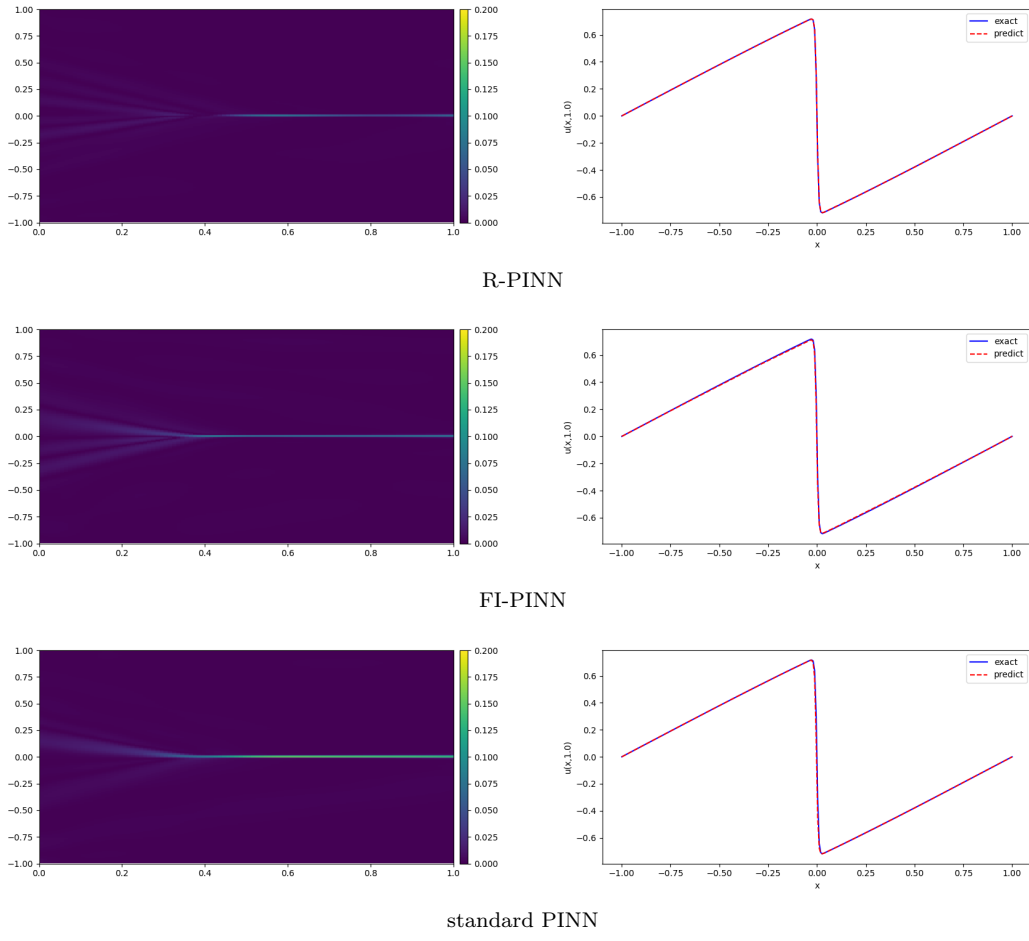


Fig. 8: The prediction err (left) and the cross section at  $t = 1$  (right) of three methods solving Burgers' equation.

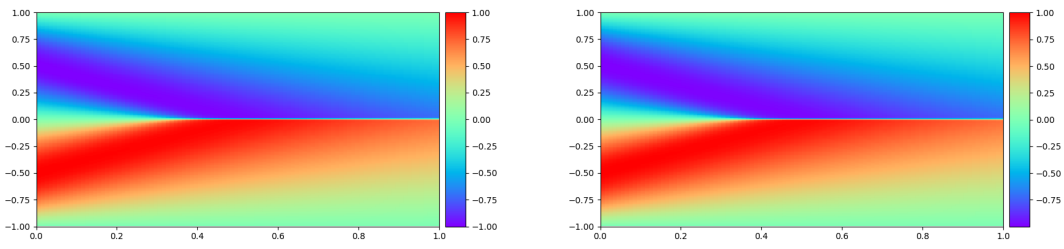


Fig. 9: The predicted solution (R-PINN at the left and FI-PINN at the right).

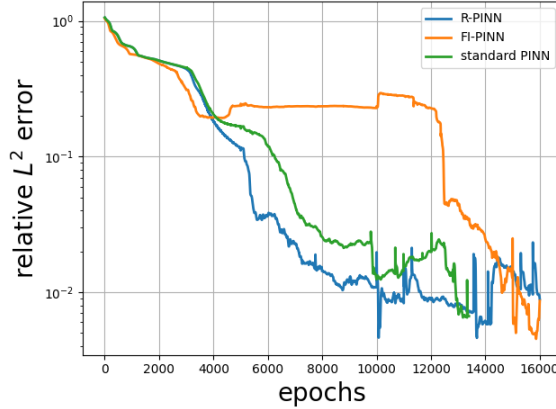


Fig. 10: The relative  $L^2$  errors of three methods in the optimization process of solving Burgers' equation.

$N_{iter}$	R-PINN			FI-PINN			standard PINN	
	Relative $L^2$	$L^\infty$	$N_2$	Relative $L^2$	$L^\infty$	$N_2$	Relative $L^2$	$L^\infty$
1	0.6778	0.1228	150	0.4372	0.4845	750	0.7912	0.6651
2	0.1202	0.0198	150	0.5220	0.3429	1500	0.8020	0.6475
3	0.1080	0.0259	150	0.4773	0.2233	2250	0.8012	0.6483
4	0.0840	0.0127	150	0.3969	0.2263	3000	0.8342	0.6625

Table 3: The relative  $L^2$  error and  $L^\infty$  error by two methods solving two-dimensional problem with two peaks.

the vicinities of  $(0.5, 0.5)$  and  $(-0.5, -0.5)$  with R-PINN, demonstrating the capability of our algorithm to effectively handle problems characterized by multiple regions of abrupt changes. However, the distribution of adaptive collocation points with FI-PINN seems not so effective to deal with the two peaks. The reason of it might be a truncated Gaussian distribution is used, so that problems of more than one regions with large error are difficult to handle. This problem is also reflected in the training process. Table 3 compares the relative  $L^2$  and  $L^\infty$  errors among R-PINN, FI-PINN and standard PINN during the adaptive iterations. For R-PINN, the relative  $L^2$  error reduces to 0.0840, and the  $L^\infty$  error decreases to 0.0127. In contrast, the relative  $L^2$  error associated with FI-PINN can only reach 0.3969 and the  $L^\infty$  can get to 0.2263, which is just a little bit lower than those with standard PINN. Similar trends are observed in Fig. 14, where the lowest relative  $L^2$  error for R-PINN falls below  $1 \times 10^{-1}$ .

Fig. 12 provides additional insights. The left panel illustrates the absolute errors across the entire domain, revealing significantly smaller errors for R-PINN. The middle and right panels display cross-sectional views at  $y = -0.5$  and  $y = 0.5$ , respectively, showing that the predictions from R-PINN align closely with the exact solution, whereas there are large errors near two peaks with FI-PINN and the standard PINN can only approximate the features. Finally, the numerical solutions obtained by the three methods are visualized in Fig. 13.

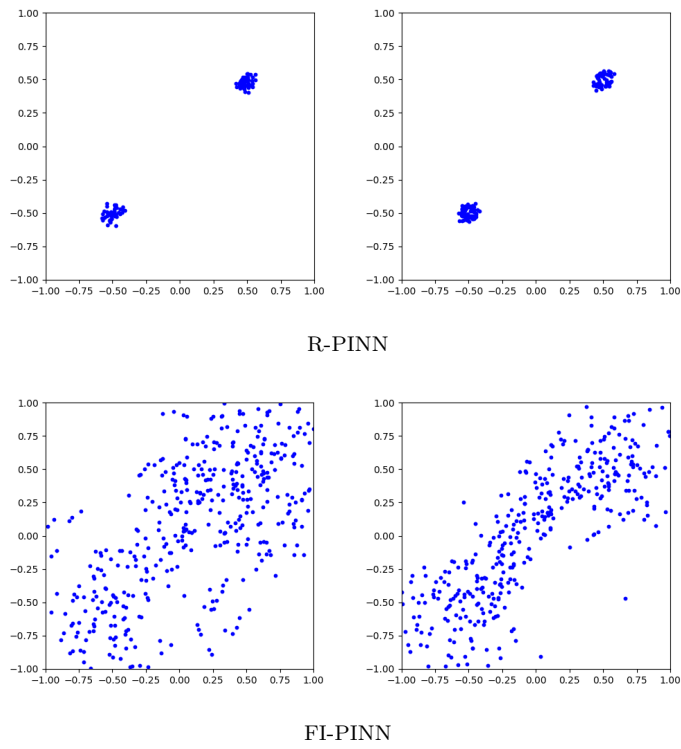


Fig. 11: The distribution of adaptive collocation points in the first two adaptive iterations of two adaptive methods solving the two-dimensional problem with two peaks.

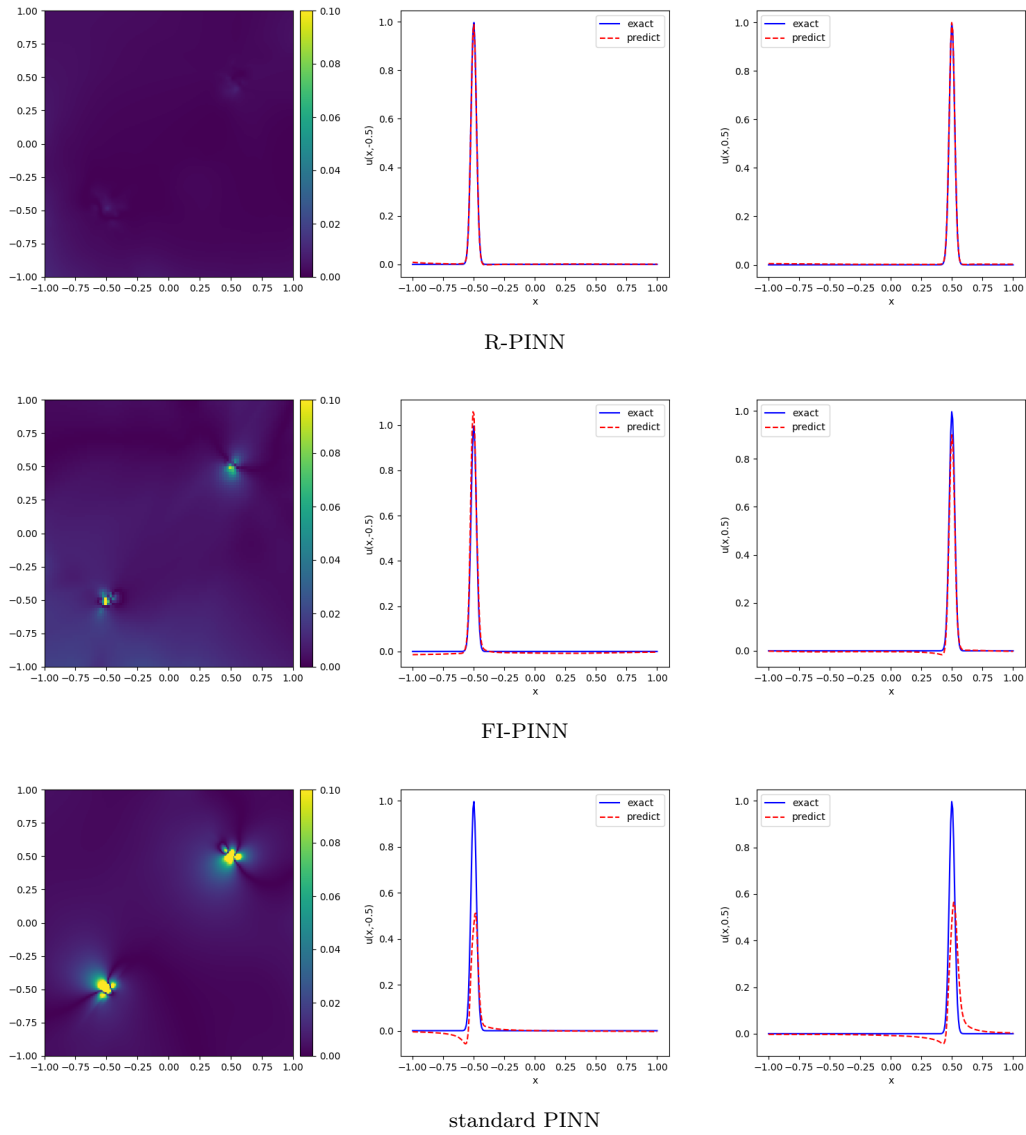


Fig. 12: The predicted err (left), the cross section at  $y = -0.5$  (middle) and the cross section at  $y = 0.5$  (right) of three methods solving the two-dimensional problem with two peaks.

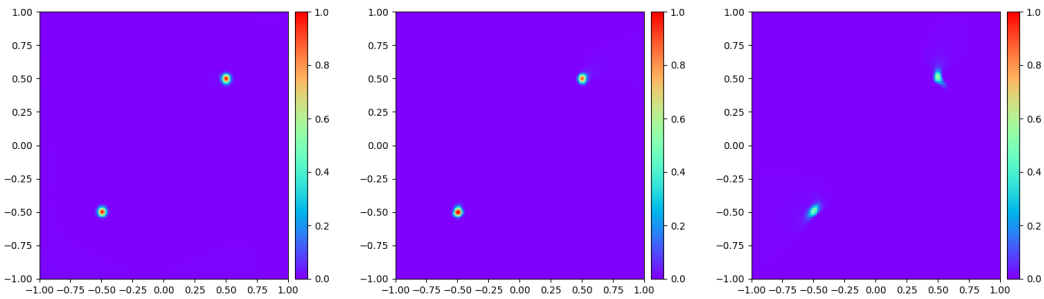


Fig. 13: The predicted solution (R-PINN at the left, FI-PINN at the middle and standard PINN at the right) of the two-dimensional problem with two peaks.

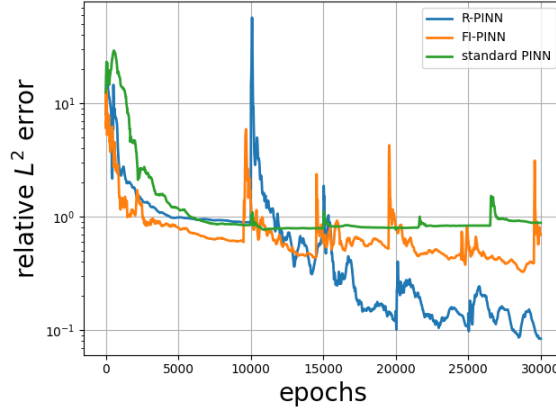


Fig. 14: The relative  $L^2$  errors of three methods in the optimization process of solving the two-dimensional problem with two peaks.

#### 4.5. Wave equation

For this test, we consider a wave equation as follow,

$$\begin{aligned} \frac{\partial^2 u}{\partial t^2} - 3 \frac{\partial^2 u}{\partial x^2} &= 0, \quad (t, x) \in [0, 6] \times [-5, 5], \\ u(0, x) &= \frac{1}{\cosh(2x)} - \frac{0.5}{\cosh(2(x-10))} - \frac{0.5}{\cosh(2(x+10))}, \\ \frac{\partial u}{\partial t}(0, x) &= 0, \\ u(t, -5) = u(t, 5) &= 0, \end{aligned} \quad (4.7)$$

where the true solution is

$$u(t, x) = \frac{0.5}{\cosh(2(x - \sqrt{3}t))} - \frac{0.5}{\cosh(2(x - 10 + \sqrt{3}t))} + \frac{0.5}{\cosh(2(x + \sqrt{3}t))} - \frac{0.5}{\cosh(2(x + 10 - \sqrt{3}t))}. \quad (4.8)$$

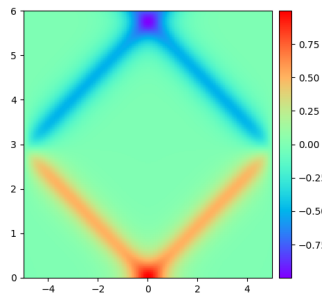


Fig. 15: The plot of the exact solution.

In this test, the R-PINN method quickly reaches its performance limit. Therefore, we adopt a single adaptive iteration process ( $M = 2$ ) and pre-train the network for 5000 iterations. We show the relative  $L^2$  errors and  $L^\infty$  errors in the Table 4. The relative  $L^2$  error

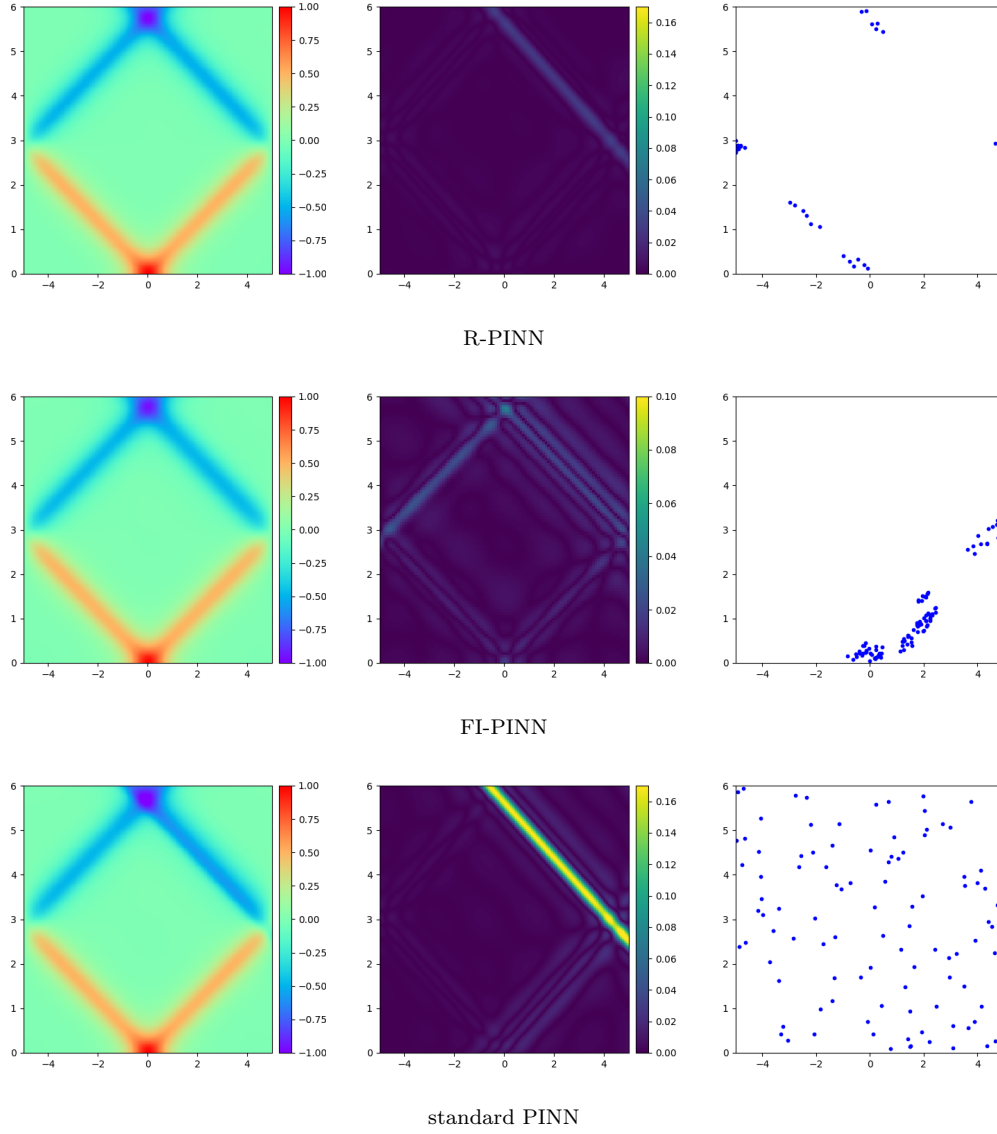


Fig. 16: The predicted solution (left), predicted error (middle) and the distribution of adaptive collocation points (right) of three methods solving the wave equation.

$N_{\text{iter}}$	R-PINN			FI-PINN			standard PINN	
	Relative $L^2$	$L^\infty$	$N_2$	Relative $L^2$	$L^\infty$	$L^2$	Relative $L^2$	$L^\infty$
1	0.0572	0.0761	100	0.1110	0.1590	500	0.3448	0.4554
2	0.0076	0.0098	100	0.0317	0.0491	1000	0.3158	0.4214

Table 4: The relative  $L^2$  error and  $L^\infty$  error by three methods solving the wave equation.

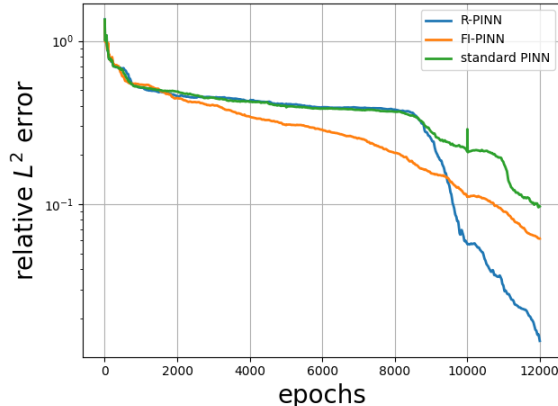


Fig. 17: The relative  $L^2$  errors of three methods in the optimization process of solving the Poisson equation the wave equation.

and  $L^\infty$  error can reach 0.0076 and 0.0098 with R-PINN, which are obviously lower than the other two methods. The detailed decreasing process is convenient to be seen in Fig. 17. The exact solution is depicted in Fig. 15. The left panel of Fig. 16 compares the predicted solutions of the three methods. The middle panel of Fig. 16 illustrates the absolute errors across the domain, showing that the errors associated with R-PINN are smaller than those with FI-PINN and standard PINN. Finally, the right panel of Fig. 16 displays the adaptive collocation points for two adaptive methods and random points for the standard PINN. From the right panel, we can see that the same problem occurs for FI-PINN when dealing with multiple large errors region, so it can't handle well.

## 5. Conclusion

In this paper, we present recovery-type a-posteriori estimator enhanced adaptive PINN that combines the PINN with a recovery type estimator which is popularly used in the adaptive finite element method. Our innovation lies in the use of the recovery-type a-posteriori error estimator, which is different from the residual of PINNs, and the design of a tailored sampling method R-AD. We test the performance of R-PINN in several PDE problems with sharp or singular solutions, which normal PINN struggles to handle effectively. The results demonstrate that R-PINN achieves significant improvements over normal PINN. More studies can be done to analyze the performance of R-PINN for more complex problems and we shall focus on and analyze these issues in our future work.

## References

- [1] M. Raissi, P. Perdikaris, G. E. Karniadakis, Physics-informed neural networks: A deep learning framework for solving forward and inverse problems involving nonlinear partial differential equations, *Journal of Computational Physics* 378 (2019) 686–707. doi:[https://10.1016/j.jcp.2018.10.045](https://doi.org/10.1016/j.jcp.2018.10.045).

- [2] M. Raissi, A. Yazdani, G. E. Karniadakis, Hidden fluid mechanics: Learning velocity and pressure fields from flow visualizations, *Science* 367 (2020) 1026–1030. doi:<https://doi.org/10.1126/science.aaw4741>.
- [3] Y. Chen, L. Lu, G. E. Karniadakis, L. Dal Negro, Physics-informed neural networks for inverse problems in nano-optics and metamaterials, *Optics Express* 28 (2020) 11618–11633. doi:<https://doi.org/10.1364/OE.384875>.
- [4] G. Pang, L. Lu, G. E. Karniadakis, fPINNs: Fractional physics-informed neural networks, *SIAM Journal on Scientific Computing* 41 (2019) A2603–A2626. doi:<https://doi.org/10.1137/18M1229845>.
- [5] D. Zhang, L. Lu, L. Guo, G. E. Karniadakis, Quantifying total uncertainty in physics-informed neural networks for solving forward and inverse stochastic problems, *Journal of Computational Physics* 397 (2019) 108850. doi:<https://doi.org/10.1016/j.jcp.2019.07.048>.
- [6] L. Guo, H. Wu, T. Zhou, Normalizing field flows: Solving forward and inverse stochastic differential equations using physics-informed flow models, *Journal of Computational Physics* 461 (2022) 111202. doi:<https://doi.org/10.1016/j.jcp.2022.111202>.
- [7] S. Wang, Y. Teng, P. Perdikaris, Understanding and mitigating gradient flow pathologies in physics-informed neural networks, *SIAM Journal on Scientific Computing* 43 (2021) A3055–A3081. doi:<https://doi.org/10.1137/20M1318043>.
- [8] L. Lu, R. Pestourie, W. Yao, Z. Wang, F. Verdugo, S. G. Johnson, Physics-informed neural networks with hard constraints for inverse design, *SIAM Journal on Scientific Computing* 43 (2021) B1105–B1132. doi:<https://doi.org/10.1137/21M1397908>.
- [9] S. Wang, X. Yu, P. Perdikaris, When and why PINNs fail to train: A neural tangent kernel perspective, *Journal of Computational Physics* 449 (2022) 110768. doi:<https://doi.org/10.1016/j.jcp.2021.110768>.
- [10] Y. Gu, H. Yang, C. Zhou, Selectnet: Self-paced learning for high-dimensional partial differential equations, *Journal of Computational Physics* 441 (2021) 110444. doi:<https://doi.org/10.1016/j.jcp.2021.110444>.
- [11] X. Meng, Z. Li, D. Zhang, G. E. Karniadakis, PPINN: Parareal physics-informed neural network for time-dependent PDEs, *Computer Methods in Applied Mechanics and Engineering* 370 (2020) 113250. doi:<https://doi.org/10.1016/j.cma.2020.113250>.
- [12] K. Shukla, A. D. Jagtap, G. E. Karniadakis, Parallel physics-informed neural networks via domain decomposition, *Journal of Computational Physics* 447 (2021) 110683. doi:<https://doi.org/10.1016/j.jcp.2021.110683>.
- [13] A. D. Jagtap, G. E. Karniadakis, Extended physics-informed neural networks (XPINNs): A generalized space-time domain decomposition based deep learning framework for nonlinear partial differential equations, *Communications in Computational Physics* 28 (2020). doi:<https://doi.org/10.4208/cicp.oa-2020-0164>.

- [14] A. F. Psaros, K. Kawaguchi, G. E. Karniadakis, Meta-learning PINN loss functions, *Journal of Computational Physics* 458 (2022) 111121. doi:<https://doi.org/10.1016/j.jcp.2022.111121>.
- [15] L. D. McClenny, U. M. Braga-Neto, Self-adaptive physics-informed neural networks, *Journal of Computational Physics* 474 (2023) 111722. doi:<https://doi.org/10.1016/j.jcp.2022.111722>.
- [16] P. L. Lagari, L. H. Tsoukalas, S. Safarkhani, I. E. Lagaris, Systematic construction of neural forms for solving partial differential equations inside rectangular domains, subject to initial, boundary and interface conditions, *International Journal on Artificial Intelligence Tools* 29 (2020) 2050009. doi:<https://doi.org/10.1142/S0218213020500098>.
- [17] S. Dong, N. Ni, A method for representing periodic functions and enforcing exactly periodic boundary conditions with deep neural networks, *Journal of Computational Physics* 435 (2021) 110242. doi:<https://doi.org/10.1016/j.jcp.2021.110242>.
- [18] L. Lu, X. Meng, Z. Mao, G. E. Karniadakis, DeepXDE: A deep learning library for solving differential equations, *SIAM Review* 63 (2021) 208–228. doi:<https://doi.org/10.1137/19M1274067>.
- [19] C. Wu, M. Zhu, Q. Tan, Y. Kartha, L. Lu, A comprehensive study of non-adaptive and residual-based adaptive sampling for physics-informed neural networks, *Computer Methods in Applied Mechanics and Engineering* 403 (2023) 115671. doi:<https://doi.org/10.1016/j.cma.2022.115671>.
- [20] Z. Gao, L. Yan, T. Zhou, Failure-informed adaptive sampling for PINNs, *SIAM Journal on Scientific Computing* 45 (2023) A1971–A1994. doi:<https://doi.org/10.1137/22M1527763>.
- [21] M. A. Nabian, R. J. Gladstone, H. Meidani, Efficient training of physics-informed neural networks via importance sampling, *Computer-Aided Civil and Infrastructure Engineering* 36 (2021) 962–977. doi:<https://doi.org/10.1111/mice.12685>.
- [22] W. Gao, C. Wang, Active learning based sampling for high-dimensional nonlinear partial differential equations, *Journal of Computational Physics* 475 (2023) 111848. doi:<https://doi.org/10.1016/j.jcp.2022.111848>.
- [23] S. Zeng, Z. Zhang, Q. Zou, Adaptive deep neural networks methods for high-dimensional partial differential equations, *Journal of Computational Physics* 463 (2022) 111232. doi:<https://doi.org/10.1016/j.jcp.2022.111232>.
- [24] J. M. Hanna, J. V. Aguado, S. Comas-Cardona, R. Askri, D. Borzacchiello, Residual-based adaptivity for two-phase flow simulation in porous media using physics-informed neural networks, *Computer Methods in Applied Mechanics and Engineering* 396 (2022) 115100. doi:<https://doi.org/10.1016/j.cma.2022.115100>.

- [25] I. Babuška, W. C. Rheinboldt, Error estimates for adaptive finite element computations, *SIAM Journal on Numerical Analysis* 15 (1978) 736–754. doi:<https://doi.org/10.1137/0715049>.
- [26] I. Babuška, W. C. Rheinboldt, A-posteriori error estimates for the finite element method, *International Journal for Numerical Methods in Engineering* 12 (1978) 1597–1615. doi:<https://doi.org/10.1002/nme.1620121010>.
- [27] O. C. Zienkiewicz, J. Z. Zhu, A simple error estimator and adaptive procedure for practical engineering analysis, *International Journal for Numerical Methods in Engineering* 24 (1987) 337–357. doi:<https://doi.org/10.1002/nme.1620240206>.
- [28] O. C. Zienkiewicz, J. Z. Zhu, The superconvergent patch recovery and a posteriori error estimates. part 1: The recovery technique, *International Journal for Numerical Methods in Engineering* 33 (1992) 1331–1364. doi:<https://doi.org/10.1002/nme.1620330702>.
- [29] O. C. Zienkiewicz, J. Z. Zhu, The superconvergent patch recovery and a posteriori error estimates. part 2: Error estimates and adaptivity, *International Journal for Numerical Methods in Engineering* 33 (1992) 1365–1382. doi:<https://doi.org/10.1002/nme.1620330703>.
- [30] H. Guo, X. Zhuang, P. Chen, N. Alajlan, T. Rabczuk, Analysis of three-dimensional potential problems in non-homogeneous media with physics-informed deep collocation method using material transfer learning and sensitivity analysis, *Engineering with Computers* 38 (2022) 5423–5444. doi:<https://doi.org/10.1007/s00366-022-01633-6>.
- [31] M. D. McKay, R. J. Beckman, W. J. Conover, A comparison of three methods for selecting values of input variables in the analysis of output from a computer code, *Technometrics* 42 (2000) 55–61. doi:<https://doi.org/10.2307/1268522>.
- [32] M. Stein, Large sample properties of simulations using Latin hypercube sampling, *Technometrics* 29 (1987) 143–151. doi:<https://doi.org/10.2307/1269769>.
- [33] J. H. Halton, On the efficiency of certain quasi-random sequences of points in evaluating multi-dimensional integrals, *Numerische Mathematik* 2 (1960) 84–90. doi:<https://doi.org/10.1007/BF01386213>.
- [34] J. Hammersley, *Monte Carlo Methods*, Springer Science & Business Media, 2013.
- [35] I. M. Sobol’, On the distribution of points in a cube and the approximate evaluation of integrals, *Zhurnal Vychislitel’noi Matematiki i Matematicheskoi Fiziki* 7 (1967) 784–802. doi:[https://doi.org/10.1016/0041-5553\(67\)90144-9](https://doi.org/10.1016/0041-5553(67)90144-9).
- [36] R. E. Bank, A. Weiser, Some a posteriori error estimators for elliptic partial differential equations, *Mathematics of Computation* 44 (1985) 283–301. doi:<https://doi.org/10.2307/2007953>.
- [37] H. Wei, Y. Huang, FEALPy: Finite element analysis library in python. <https://github.com/weihuayi/fealpy>, Xiangtan University, 2017-2022. URL: <https://github.com/weihuayi/fealpy>.